

# Measurement of the $^{140}\text{Ce}(n, \gamma)$ Cross Section at n\_TOF and Its Astrophysical Implications for the Chemical Evolution of the Universe

---

(n\_TOF Collaboration) Amaducci, S.; Colonna, N.; Cosentino, L.; Cristallo, S.; Finocchiaro, P.; Krtićka, M.; Massimi, C.; Mastro marco, M.; Mazzone, A.; Maugeri, E. A.; ...

Source / Izvornik: **Physical Review Letters, 2024, 132**

Journal article, Published version

Rad u časopisu, Objavljena verzija rada (izdavačev PDF)

<https://doi.org/10.1103/PhysRevLett.132.122701>

Permanent link / Trajna poveznica: <https://um.nsk.hr/um:nbn:hr:217:107103>

Rights / Prava: [Attribution 4.0 International](#) / [Imenovanje 4.0 međunarodna](#)

Download date / Datum preuzimanja: **2024-12-18**



Repository / Repozitorij:

[Repository of the Faculty of Science - University of Zagreb](#)



## Measurement of the $^{140}\text{Ce}(n,\gamma)$ Cross Section at n\_TOF and Its Astrophysical Implications for the Chemical Evolution of the Universe

S. Amaducci<sup>1</sup>, N. Colonna,<sup>2</sup> L. Cosentino,<sup>1</sup> S. Cristallo,<sup>3,4</sup> P. Finocchiaro,<sup>1</sup> M. Krtička,<sup>5</sup> C. Massimi,<sup>6,7</sup> M. Mastromarco,<sup>8</sup> A. Mazzone,<sup>2,9</sup> E. A. Maugeri,<sup>10</sup> A. Mengoni,<sup>6,11</sup> I. U. Roederer,<sup>12,13,14</sup> O. Straniero,<sup>3,15</sup> S. Valenta,<sup>5</sup> D. Vescovi,<sup>3,4</sup> O. Aberle,<sup>8</sup> V. Alcayne,<sup>16</sup> J. Andrzejewski,<sup>17</sup> L. Audouin,<sup>18</sup> V. Babiano-Suarez,<sup>19</sup> M. Bacak,<sup>8,20,21</sup> M. Barbagallo,<sup>8,2</sup> S. Bennett,<sup>22</sup> E. Berthoumieux,<sup>21</sup> J. Billowes,<sup>22</sup> D. Bosnar,<sup>23</sup> A. Brown,<sup>24</sup> M. Busso,<sup>4,25</sup> M. Caamaño,<sup>26</sup> L. Caballero-Ontanaya,<sup>19</sup> F. Calviño,<sup>27</sup> M. Calviani,<sup>8</sup> D. Cano-Ott,<sup>16</sup> A. Casanovas,<sup>27</sup> F. Cerutti,<sup>8</sup> E. Chiaveri,<sup>8,22</sup> G. Cortés,<sup>27</sup> M. A. Cortés-Giraldo,<sup>28</sup> L. A. Damone,<sup>2,29</sup> P. J. Davies,<sup>22</sup> M. Diakaki,<sup>30,8</sup> M. Dietz,<sup>31</sup> C. Domingo-Pardo,<sup>19</sup> R. Dressler,<sup>10</sup> Q. Ducasse,<sup>32</sup> E. Dupont,<sup>21</sup> I. Durán,<sup>26</sup> Z. Eleme,<sup>33</sup> B. Fernández-Domínguez,<sup>26</sup> A. Ferrari,<sup>8</sup> V. Furman,<sup>34</sup> K. Göbel,<sup>35</sup> R. Garg,<sup>31</sup> A. Gawlik-Ramieęa,<sup>17</sup> S. Gilardoni,<sup>8</sup> I. F. Gonçalves,<sup>36</sup> E. González-Romero,<sup>16</sup> C. Guerrero,<sup>28</sup> F. Gunsing,<sup>21</sup> H. Harada,<sup>37</sup> S. Heintz,<sup>10</sup> J. Heyse,<sup>38</sup> D. G. Jenkins,<sup>24</sup> A. Junghans,<sup>39</sup> F. Käppeler,<sup>40,\*</sup> Y. Kadi,<sup>8</sup> A. Kimura,<sup>37</sup> I. Knapová,<sup>5</sup> M. Kokkoris,<sup>30</sup> Y. Kopatch,<sup>34</sup> D. Kurtulgil,<sup>35</sup> I. Ladarescu,<sup>19</sup> C. Lederer-Woods,<sup>31</sup> H. Leeb,<sup>20</sup> J. Lerendegui-Marco,<sup>28</sup> S. J. Lonsdale,<sup>31</sup> D. Macina,<sup>8</sup> A. Manna,<sup>6,7</sup> T. Martínez,<sup>16</sup> A. Masi,<sup>8</sup> P. Mastinu,<sup>41</sup> E. Mendoza,<sup>16</sup> V. Michalopoulou,<sup>30,8</sup> P. M. Milazzo,<sup>42</sup> F. Mingrone,<sup>8</sup> J. Moreno-Soto,<sup>21</sup> A. Musumarra,<sup>43,44</sup> A. Negret,<sup>45</sup> R. Nolte,<sup>32</sup> F. Ogállar,<sup>46</sup> A. Oprea,<sup>45</sup> N. Patronis,<sup>33</sup> A. Pavlik,<sup>47</sup> J. Perkowski,<sup>17</sup> C. Petrone,<sup>45</sup> L. Piersanti,<sup>3,4</sup> E. Pirovano,<sup>32</sup> I. Porras,<sup>46</sup> J. Praena,<sup>46</sup> J. M. Quesada,<sup>28</sup> D. Ramos-Doval,<sup>18</sup> T. Rauscher,<sup>48,49</sup> R. Reifarth,<sup>35</sup> D. Rochman,<sup>10</sup> C. Rubbia,<sup>8</sup> M. Sabaté-Gilarte,<sup>28,8</sup> A. Saxena,<sup>50</sup> P. Schillebeeckx,<sup>38</sup> D. Schumann,<sup>10</sup> A. Sekhar,<sup>22</sup> A. G. Smith,<sup>22</sup> N. V. Sosnin,<sup>22</sup> P. Sprung,<sup>10</sup> A. Stamatopoulos,<sup>30</sup> G. Tagliente,<sup>2</sup> J. L. Tain,<sup>19</sup> A. Tarifeño-Saldivia,<sup>19</sup> L. Tassan-Got,<sup>8,30,18</sup> Th. Thomas,<sup>35</sup> P. Torres-Sánchez,<sup>46</sup> A. Tsinganis,<sup>8</sup> J. Ulrich,<sup>10</sup> S. Urluss,<sup>39,8</sup> G. Vannini,<sup>6,7</sup> V. Variale,<sup>2</sup> P. Vaz,<sup>36</sup> A. Ventura,<sup>6</sup> V. Vlachoudis,<sup>8</sup> R. Vlastou,<sup>30</sup> A. Wallner,<sup>51</sup> P. J. Woods,<sup>31</sup> T. Wright,<sup>22</sup> and P. Žugec<sup>23</sup>

(n\_TOF Collaboration)

<sup>1</sup>INFN Laboratori Nazionali del Sud, Catania, Italy

<sup>2</sup>Istituto Nazionale di Fisica Nucleare, Sezione di Bari, Italy

<sup>3</sup>Istituto Nazionale di Astrofisica - Osservatorio Astronomico d'Abruzzo, Italy

<sup>4</sup>Istituto Nazionale di Fisica Nucleare, Sezione di Perugia, Italy

<sup>5</sup>Charles University, Prague, Czech Republic

<sup>6</sup>Istituto Nazionale di Fisica Nucleare, Sezione di Bologna, Italy

<sup>7</sup>Dipartimento di Fisica e Astronomia, Università di Bologna, Italy

<sup>8</sup>European Organization for Nuclear Research (CERN), Switzerland

<sup>9</sup>Consiglio Nazionale delle Ricerche, Bari, Italy

<sup>10</sup>Paul Scherrer Institut (PSI), Villigen, Switzerland

<sup>11</sup>Agenzia nazionale per le nuove tecnologie, l'energia e lo sviluppo economico sostenibile (ENEA), Italy

<sup>12</sup>Department of Physics, North Carolina State University, Raleigh, North Carolina 27695, USA

<sup>13</sup>Department of Astronomy, University of Michigan, Ann Arbor, Michigan 48109, USA

<sup>14</sup>Joint Institute for Nuclear Astrophysics—Center for the Evolution of the Elements (JINA-CEE), USA

<sup>15</sup>INFN Sezione Napoli, Napoli, Italy

<sup>16</sup>Centro de Investigaciones Energéticas Medioambientales y Tecnológicas (CIEMAT), Spain

<sup>17</sup>University of Lodz, Poland

<sup>18</sup>Institut de Physique Nucléaire, CNRS-IN2P3, Univ. Paris-Sud, Université Paris-Saclay, F-91406 Orsay Cedex, France

<sup>19</sup>Istituto de Física Corpuscular, CSIC - Universidad de Valencia, Spain

<sup>20</sup>TU Wien, Atominstitut, Stadionallee 2, 1020 Wien, Austria

<sup>21</sup>CEA Irfu, Université Paris-Saclay, F-91191 Gif-sur-Yvette, France

<sup>22</sup>University of Manchester, United Kingdom

<sup>23</sup>Department of Physics, Faculty of Science, University of Zagreb, Zagreb, Croatia

<sup>24</sup>University of York, United Kingdom

<sup>25</sup>Dipartimento di Fisica e Geologia, Università di Perugia, Italy


<sup>26</sup>IGFAE—Universidad de Santiago de Compostela, Spain

<sup>27</sup>Universitat Politècnica de Catalunya, Spain

<sup>28</sup>Universidad de Sevilla, Spain

<sup>29</sup>Dipartimento Interateneo di Fisica, Università degli Studi di Bari, Italy

<sup>30</sup>National Technical University of Athens, Greece

<sup>31</sup>*School of Physics and Astronomy, University of Edinburgh, United Kingdom*<sup>32</sup>*Physikalisch-Technische Bundesanstalt (PTB), Bundesallee 100, 38116 Braunschweig, Germany*<sup>33</sup>*University of Ioannina, Greece*<sup>34</sup>*Affiliated with an institute or an international laboratory covered by a cooperation agreement with CERN*<sup>35</sup>*Goethe University Frankfurt, Germany*<sup>36</sup>*Instituto Superior Técnico, Lisbon, Portugal*<sup>37</sup>*Japan Atomic Energy Agency (JAEA), Tokai-Mura, Japan*<sup>38</sup>*European Commission, Joint Research Centre (JRC), Geel, Belgium*<sup>39</sup>*Helmholtz-Zentrum Dresden-Rossendorf, Germany*<sup>40</sup>*Karlsruhe Institute of Technology, Campus North, IKP, 76021 Karlsruhe, Germany*<sup>41</sup>*INFN Laboratori Nazionali di Legnaro, Italy*<sup>42</sup>*Istituto Nazionale di Fisica Nucleare, Sezione di Trieste, Italy*<sup>43</sup>*Istituto Nazionale di Fisica Nucleare, Sezione di Catania, Italy*<sup>44</sup>*Department of Physics and Astronomy, University of Catania, Italy*<sup>45</sup>*Horia Hulubei National Institute of Physics and Nuclear Engineering, Romania*<sup>46</sup>*University of Granada, Spain*<sup>47</sup>*University of Vienna, Faculty of Physics, Vienna, Austria*<sup>48</sup>*Department of Physics, University of Basel, Switzerland*<sup>49</sup>*Centre for Astrophysics Research, University of Hertfordshire, United Kingdom*<sup>50</sup>*Bhabha Atomic Research Centre (BARC), India*<sup>51</sup>*Australian National University, Canberra, Australia* (Received 30 June 2023; revised 9 November 2023; accepted 31 January 2024; published 21 March 2024)

$^{140}\text{Ce}(n, \gamma)$  is a key reaction for slow neutron-capture (*s*-process) nucleosynthesis due to being a bottleneck in the reaction flow. For this reason, it was measured with high accuracy (uncertainty  $\approx 5\%$ ) at the n\_TOF facility, with an unprecedented combination of a high purity sample and low neutron-sensitivity detectors. The measured Maxwellian averaged cross section is up to 40% higher than previously accepted values. Stellar model calculations indicate a reduction around 20% of the *s*-process contribution to the Galactic cerium abundance and smaller sizeable differences for most of the heavier elements. No variations are found in the nucleosynthesis from massive stars.

DOI: [10.1103/PhysRevLett.132.122701](https://doi.org/10.1103/PhysRevLett.132.122701)

*Introduction.*—In the Universe, roughly half of the atomic nuclei heavier than iron are synthesized by the slow (*s*) neutron-capture process [1,2]. The main component of this process occurs in the interiors of low-mass stars, during their asymptotic giant branch (AGB) phase [3–6]. In this context, nuclei with closed neutron shells play a crucial role due to their low neutron-capture cross sections, which impact heavy element yields from *s*-process enriched stars. In particular, the low neutron-capture cross section of the neutron-magic nucleus  $^{140}_{58}\text{Ce}$  represents a bottleneck for the neutron-capture path. As a consequence, its abundance is significantly higher when compared to heavier nuclei. This is evident in the Solar System abundance distribution, where the three peaks corresponding to the neutron-magic numbers  $N = 50, 82, \text{ and } 126$  are well pronounced. The  $^{140}\text{Ce}(n, \gamma)$  reaction

represents the main destruction process of this element, since  $^{140}\text{Ce}$  is the most abundant cerium isotope (89%). The other stable isotope ( $^{142}\text{Ce}$ ) is almost bypassed by the *s* process due to the presence of the unstable  $^{141}\text{Ce}$  (which decays to  $^{141}\text{Pr}$  with  $t_{1/2} = 32.5$  d).

Among the neutron-magic nuclei, cerium is particularly intriguing because of a significant discrepancy (as high as 30%) between abundance predictions from nucleosynthesis calculations and spectroscopic observations of *s*-process enriched stars belonging to the Galactic globular cluster M22 [7]. In contrast, an excellent agreement is observed for the abundances of the nearby elements belonging to the second *s*-process peak, i.e., Ba, La, Nd, and Sm (Fig. 1), which makes it unlikely that the cerium discrepancy could be ascribed to shortcomings in the stellar models [7]. We note that the abundances are derived from high resolution spectra, characterized by extremely small observational errors [8].

A possible solution to this disagreement might be ascribed to an overestimation of the  $^{140}\text{Ce}$  Maxwellian averaged neutron-capture cross section (MACS) at stellar temperatures, corresponding to  $kT$  values from  $\sim 8$  to  $\sim 35$  keV. The  $^{140}\text{Ce}$  MACS values available in

---

*Published by the American Physical Society under the terms of the Creative Commons Attribution 4.0 International license. Further distribution of this work must maintain attribution to the author(s) and the published article's title, journal citation, and DOI. Open access publication funded by CERN.*

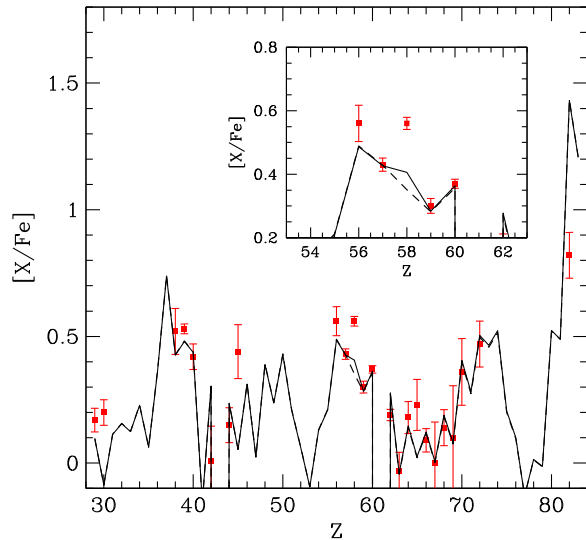


FIG. 1. Comparison between theoretical predictions and average observed abundances in  $s$ -process enhanced second-generation stars of the globular cluster M22. The red squares represent the average  $s$ -process overabundance with respect to iron (we adopt the standard spectroscopic notation:  $\{[A/B] = \log[N(A)_{\text{Star}}/N(A)_{\text{Sun}}] - \log[N(B)_{\text{Star}}/N(B)_{\text{Sun}}]\}$ ). The solid and the dashed lines show the results of the nucleosynthesis models obtained by adopting the KADoNiS0.3 and the new  $n_{\text{TOF}}$   $^{140}\text{Ce}(n, \gamma)$  reaction rate, respectively. See Straniero *et al.* [7] for more details.

the Karlsruhe Astrophysical Database of Nucleosynthesis in Stars (KADoNiS) [9] strongly relied on the activation measurement at  $kT = 25$  keV performed by Käppeler *et al.* [10], who obtained a value of  $12.0 \pm 0.4$  mb. The values at lower and higher  $kT$  were extrapolated according to statistical models based on Hauser-Feshbach theory. Other activation measurements present in literature (see [9] for more details) provide inconsistent values of the MACS at  $kT = 25$  keV, ranging from  $7.3 \pm 4.0$  to  $13.9 \pm 1.0$  mb. Note that the calculations presented in Fig. 1 were obtained using KADoNiS v0.3.

The only  $^{140}\text{Ce}(n, \gamma)$  cross section measurement performed with the time-of-flight technique and a highly enriched sample is from Harnhood *et al.* [11] in the energy range between 10 and 100 keV and with a very coarse binning (7 bins). Furthermore, this interval did not include the first resonances, which provides a significant contribution to the MACS for low  $kT$ . In particular the first resonance at 2.5 keV contributes to about 18% of the MACS for  $kT = 5$  keV. A time-of-flight measurement in a wider energy range was performed by Musgrove *et al.* [12], but with a natural cerium sample containing 11% of  $^{142}\text{Ce}$  and  $\text{C}_6\text{F}_6$  detectors. These are well-known for their high sensitivity to the neutron background; therefore, these results can suffer of possible systematic effects. Also the total cross section measurements reported in the literature were often measured using natural

samples (e.g., [13]), with  $^{142}\text{Ce}$  providing a significant contribution due to its much higher cross section and affecting the measurement when resonance overlapped. With the aim of clarifying the astrophysical discrepancies and to provide new and high precision  $^{140}\text{Ce}(n, \gamma)$  cross section data in the energy range of interest for  $s$ -process nucleosynthesis, the  $n_{\text{TOF}}$  Collaboration performed an accurate neutron-capture measurement using a highly enriched (99.4%)  $^{140}\text{Ce}$  sample and  $\gamma$ -ray detectors with very low neutron background.

*Measurement and analysis.*—The cross section measurement of the  $^{140}\text{Ce}(n, \gamma)$  reaction was performed at the neutron beam time-of-flight facility ( $n_{\text{TOF}}$ ) at CERN, characterized by a high energy resolution, a wide energy range, and a high instantaneous [14] flux. Neutrons are produced via spallation reactions by a pulsed (7 ns RMS) proton beam of 20 GeV/c hitting a water-cooled lead target. The measurement was carried out in the experimental area EAR1, at a distance of 185 m from the neutron source. The neutron beam of intensity  $5.5 \times 10^5$  neutrons/pulse from thermal (25.3 meV) to about 1 GeV is available at  $n_{\text{TOF}}$  with an energy resolution  $\Delta E_n/E_n$  up to  $10^{-4}$ . This makes EAR1 extremely suitable for high precision measurements where very narrow structures need to be resolved. The  $^{140}\text{Ce}$  sample was produced at the Paul Scherrer Institut by sintering of  $\text{CeO}_2$  powder (total mass 12.318 g) enclosed in a polyether ether ketone case 1-mm thick, with a cylindrical shape and a diameter of 2 cm. Total areal density of  $^{140}\text{Ce}$  was  $1.291 \times 10^{-2}$  atoms/barn. The large quantity of  $^{140}\text{Ce}$  in combination with the extremely low presence of contaminants (0.6% of  $^{142}\text{Ce}$ ), allowed one to perform a high precision  $^{140}\text{Ce}(n, \gamma)$  cross section measurement up to 65 keV.

The experimental setup for the detection of the prompt  $\gamma$ -ray cascade emitted by the excited compound nucleus consists of four liquid scintillators coupled to photomultipliers. The detectors were placed at  $125^\circ$  with respect to the beam direction, in order to minimize the sensitivity to the anisotropic  $\gamma$ -ray emission and to the background produced by the in-beam  $\gamma$  rays scattered by the sample [15]. The use of deuterated benzene ( $\text{C}_6\text{D}_6$ ) as scintillator material, and of carbon fiber for the detector housing and the supports, minimizes the background induced by scattered neutrons. The experimental setup was complemented by a silicon neutron flux monitor (referred to as SiMon detector [16]). Finally, a gold sample was used to normalize the neutron-capture data and to calibrate the flight-path length, exploiting the  $^{197}\text{Au}(n, \gamma)$  reaction.

The well-established pulse height weighting technique [17] was applied to extract the experimental yield as a function of the neutron energy. The application of this technique required detailed Monte Carlo simulations of the detection system, performed using the simulation package

Geant4 [18]. The experimental yield is obtained by the expression:

$$Y_{\text{exp}}(E_n) = N \frac{C_w(E_n) - B_w(E_n)}{\varepsilon(E_n)\phi(E_n)}, \quad (1)$$

where  $C_w$  are the weighted counts and  $B_w$  the weighted background. The other quantities depending on the neutron energy are the neutron flux on the target,  $\phi$ , and the cascade detection efficiency  $\varepsilon(E_n)$ , that is proportional to the excitation energy  $S_n + E_n$ . Finally,  $N$  represents the normalization factor, which includes geometrical quantities not depending on  $E_n$ , such as the sample area and the beam interception factor. The value of  $N$  was determined by means of the saturated resonance at 4.9 eV in the Au capture cross section [19].

The flight-path length was measured from the resonances of the  $^{197}\text{Au}(n, \gamma)$  reaction below 2 keV, as provided by the ENDF/B-VIII.0 library [20]. Because of the combination of the massive sample and the extremely low capture cross section of  $^{140}\text{Ce}$ , the background is dominated by scattered neutrons. This was initially deduced by comparing the total yield in the valley between resonances with that predicted by the JENDL-5 library [21] and a dummy sample. Then, it was further verified by studying the effect of black resonances using neutron absorbers. The background was estimated by a first order polynomial fit of the experimental yield in the valleys between the  $^{140}\text{Ce}$  resonances, where the background is about 3 orders of magnitude higher compared to the  $^{140}\text{Ce}$  capture events.

The resonance analysis was performed using the R-matrix code SAMMY. The n\_TOF capture data were combined with the transmission data set measured by Guber and collaborators [22] in order to provide additional constraints on the scattering width. In total, 81 of the 102 resonances in the library JENDL-5 below  $E_n = 65$  keV were fitted. Above this value the resonances are very small and the statistics is not sufficient to produce reliable fits. Four resonances not included in the libraries were identified in the analyzed energy interval.

Adopting the Reich-Moore formalism, each resonance is described in terms of the neutron energy  $E_n$  and of the two reaction width. The most relevant quantity for the MACS is the resonance strength, usually expressed in the form of the capture kernel

$$K = g \frac{\Gamma_\gamma \Gamma_n}{\Gamma_\gamma + \Gamma_n}, \quad (2)$$

where  $g$  is the spin statistical factor and  $\Gamma_\gamma$  and  $\Gamma_n$  the capture and scattering widths, respectively. The resonance parameters are given in the Supplemental Material [23].

The simultaneous analysis of capture and transmission data allowed for resonances with  $\Gamma_n \gg \Gamma_\gamma$  to determine the individual reaction width with high accuracy. For

resonances with  $\Gamma_n \sim \Gamma_\gamma$ , the fitted parameters present a strong (generally negative) correlation, allowing one to determine only their capture kernels as defined in Eq. (2). Nevertheless, these are the relevant quantities needed to calculate the MACS. In addition to the kernel determination, the shape of the absorption dips in the transmission data allowed to confirm the spin-parity assignments in the JENDL-5 library. This is particularly effective for the parity, which produces a strongly asymmetrical (+) or nearly symmetrical (−) structure, whilst the shape is less dependent on the spin. The three possible spin-parity hypotheses (namely  $1/2^+$ ,  $1/2^-$ , and  $3/2^-$ ) were evaluated on the basis of the  $\chi^2/\text{NDF}$  (where NDF indicates the number of degrees of freedom) between the transmission data and the resulting SAMMY fit. This allowed us to assign the parity of 17 resonances; in three of them the parity assignment was modified. As an example, Fig. 2 shows the transmission data together with the fit calculated for the first resonance, reported as  $1/2^+$  in the nuclear libraries and modified into  $1/2^-$  in this work.

For the resonances not fitted in this work, the energy and  $\Gamma_n$  of JENDL-5 were adopted, using the average  $\Gamma_\gamma$  derived from the basis of the n\_TOF data (52, 42, and 51 meV for spin  $1/2^+$ ,  $1/2^-$ , and  $3/2^-$ , respectively). To meet the experimental thermal cross section value ( $510 \pm 20$  mb [24]) and produce the usual  $1/v$  behavior of the cross section, a  $s$ -wave direct radiative capture process was invoked. The alternative approach of adding a contribution from a negative resonance was also tested, providing the same results. In both cases this contribution was small for all kT relevant for the nucleosynthesis (always below 4% of the total MACS).

The n\_TOF MACS values were then obtained using the experimentally derived capture kernels for all resonances, complemented by JENDL-5 library up to 200 keV. Above 200 keV, the nonresonant contribution from the evaluated nuclear data library JENDL-5 has been adopted.

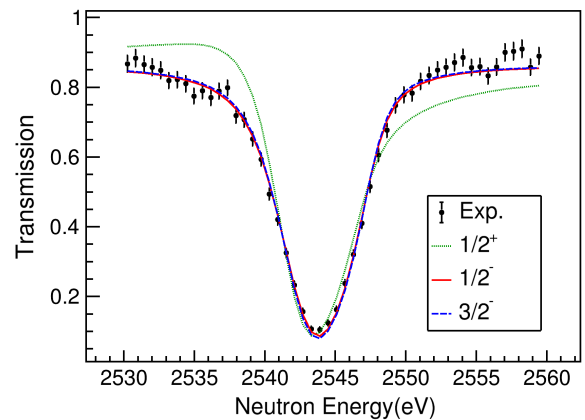


FIG. 2. Fit of the transmission data [22] with the three different spin parities. The resulting  $\chi^2/\text{NDF}$  for the  $1/2^+$ ,  $1/2^-$ , and  $3/2^-$  are, respectively, 16.8, 1.6, and 3.8.

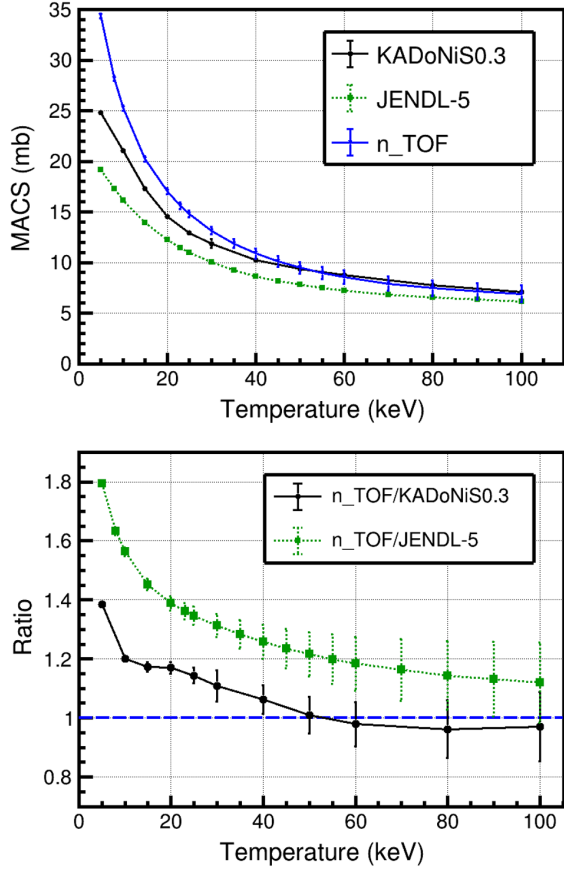


FIG. 3. Top: MACS calculated by  $n\_TOF$  compared with the values available in KADoNiS0.3 and the MACS calculated on the basis of JENDL-5 library. Bottom: ratio  $n\_TOF/KADoNiS0.3$  and  $n\_TOF/JENDL-5$ . The values of KADoNiS0.3 have been scaled by a factor 1.0785, corresponding to the recent increase in the standard  $^{197}\text{Au}(n, \gamma)$  cross section [25].

Figure 3 shows that for lower  $kT$ , the MACS from KADoNiS show large differences relative to the  $n\_TOF$  data as high as 40% for  $kT = 5$  keV and 20% at  $kT = 10$  keV. The  $n\_TOF$  MACS and the contribution of the resonances below 65 keV are reported in Table I, together with the ratio  $n\_TOF/KADoNiS0.3$ . Note that below 30 keV the contribution provided by the resonances studied in this work is always higher than 80%.

The systematic uncertainty on the MACS is dominated by those on the neutron flux in the keV energy region (2%–5%), on the pulse height weighting technique (2%) and on the flux normalization (1%).

*Astrophysical impact.*—The effects induced by the new measured MACS on the Galactic chemical evolution of cerium was explored by means of stellar models of low-mass AGB stars computed with the FUNS code [4,26,27]. The nuclear network adopted in FUNS includes all isotopes of interest to  $s$ -process nucleosynthesis (from hydrogen to lead, at the termination point of the  $s$  process). Moreover, it is directly coupled to the physical evolution of the stellar

TABLE I.  $n\_TOF$  MACS for temperatures [5,100] keV and contribution of the fitted resonance. The last column reports the ratio between  $n\_TOF$  and KADoNiS0.3.

T (keV)	$n\_TOF$ (mb)	$n\_TOF$ res.	$n\_TOF/KADoNiS0.3$
5	34.37(0.24)	96.7%	1.39(0.01)
8	28.18(0.24)	96.7%	...
10	25.26(0.25)	96.5%	1.2(0.01)
15	20.24(0.27)	94.6%	1.17(0.02)
20	17.04(0.29)	90.7%	1.17(0.02)
23	15.61(0.32)	87.7%	...
25	14.8(0.34)	85.6%	1.14(0.03)
30	13.15(0.39)	80.2%	1.11(0.05)
35	11.88(0.45)	74.7%	...
40	10.88(0.5)	69.5%	1.06(0.05)
45	10.1(0.55)	64.5%	...
50	9.47(0.59)	59.7%	1.01(0.06)
55	8.97(0.62)	55.2%	...
60	8.55(0.66)	51.1%	0.98(0.08)
70	7.92(0.72)	43.9%	...
80	7.47(0.76)	37.9%	0.96(0.10)
90	7.15(0.81)	32.7%	...
100	6.91(0.84)	28.5%	0.97(0.10)

structure. The most recent improvements made to the FUNS code are illustrated in [28–30].

The new MACS values lead, in general, to a lower cerium production in AGB stars; see Fig. 4, showing the percentage variations of heavy-isotope mass fractions for the model computed with the new MACS as compared to the reference model using KADoNiS0.3. Two models with mass equal to  $2M_{\odot}$  and metallicities representative of the Galactic disk and halo AGB stars were considered. Both models predict a significantly smaller  $^{140}\text{Ce}$  production, on average, by 20%. This has important consequences on the Galactic chemical evolution of cerium, for which an  $s$ -process contribution of about 85% to the Solar System budget was previously estimated [31]. In particular, we expect to possibly increasing its rapid ( $r$ ) process component to  $\sim 30\%$ : a more precise estimate will be determined when Galactic chemical evolutionary models, including a full set of AGB models with the new neutron capture cross section, are computed. Our result is also relevant in relation to comparison to the currently expanding number of available cerium data from spectra of Ba stars [32] and more metal-poor disk and halo stars [33]. More importantly, our new measurement will help in interpreting data provided by large spectroscopic surveys such as the GSP-Spec of Gaia DR3 (see, e.g., [34]), APOGEE DR17 [35], and GALAH DR3 [36]. As a matter of fact, the presence of systematic differences (in particular different reference scales) does not provide strong constraints on the chemical evolution of cerium. For this reason, theoretical studies aiming at reproducing the evolution of cerium abundance along the stellar disk (and thus over the temporal evolution

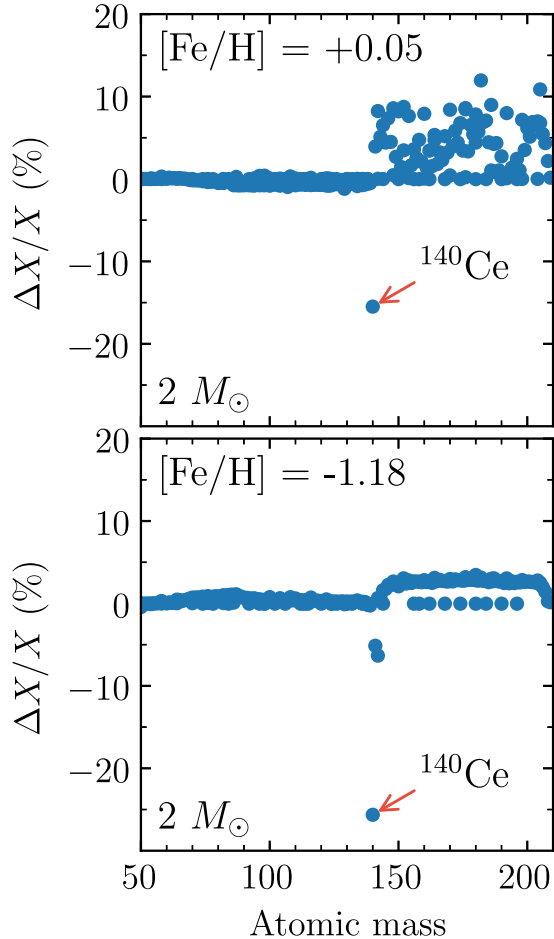


FIG. 4. Percentage differences between models computed with the new  $^{140}\text{Ce}$  MACS and the KADoNiS0.3 one. Computed models are representative of disk (upper panel) and halo (lower panel) AGB stars. As expected, the abundance of the stable  $p$ -only nuclei is unchanged. We adopted the iron abundance relative to hydrogen,  $[\text{Fe}/\text{H}]$ , as a tracer of stellar metallicity.

of the Milky Way) are essential to validate observed trends, possibly stressing the presence of potential observational biases. Another interesting feature emerging from Fig. 4 is the increased production of isotopes heavier than  $^{140}\text{Ce}$ . This fact clearly derives from the fact that  $^{140}\text{Ce}$  is a bottleneck for the production of heavier nuclei. As a result, the higher  $^{140}\text{Ce}$  MACS translates into an enhanced neutron flux through the following (heavier) isotopes. This behavior is most evident in the bottom plot of Fig. 4, where two separate distributions are present above  $A = 140$ , while in the high-metallicity model, the  $p$ -only are blended with the other isotopes. Negligible variations are found for lighter nuclei. We also evaluated the effects induced by the new MACS values on the cerium production in fast-rotating massive stars at low metallicity [37,38] by using Nu-Grid simulations [39]. We did not find sizable differences from these calculations because the old and new MACS values well agree at energies relevant for these stars.

Finally, we analyzed the problem connected to the cerium abundance measured in globular clusters. The dashed curve in Fig. 1 marks the calculated chemical distribution obtained with the new  $^{140}\text{Ce}$  MACS values. As expected, we found a slight worsening (by a few percent) of the comparison between theory and observations. As a consequence, the present data allow one to unambiguously rule out the  $^{140}\text{Ce}(n, \gamma)$  cross section as the origin of this discrepancy. It is hard to hypothesize the presence of observational biases explaining such a difference, since the abundance pattern shown in Fig. 1 results from a differential analysis of several stars with similar parameters. Additionally, lines of neighboring elements (as La or Nd) form under similar conditions and respond similarly to changes in the adopted model atmosphere. Moreover, the Ce II lines used to derive the abundances in metal-poor stars are unsaturated and corresponding atomic data are known to high precision. A fascinating, but rather uncertain, alternative hypothesis may be ascribed to the intervention of the so-called intermediate neutron capture process ( $i$  process [40]), in which unstable isotopes far from the  $\beta$  stability valley may be produced. In this case, a larger production of  $^{140}\text{Ba}$  (potentially caused by a lower neutron capture cross section) may lead to an increase of the  $^{140}\text{Ce}$  surface abundance (and eventually explain the low Pb abundances measured in these stars; see, e.g., [41]). The neutron capture of the  $^{140}\text{Ba}$  has never been measured and, thus, is extremely uncertain. Although very challenging, a measurement of this cross section would be of utmost importance, and we are currently investigating this possibility at n\_TOF.

**Conclusions.**—By combining the high resolution of the n\_TOF facility and a highly enriched sample, the  $^{140}\text{Ce}(n, \gamma)$  cross section was measured for the first time with high accuracy in the energy range of interest for the  $s$ -process nucleosynthesis. The new data highlighted high discrepancies with respect to main nuclear data libraries, providing a fundamental contribution to improve the knowledge of this cross section. The MACS calculated on the basis on the n\_TOF data is larger than that provided by the astrophysics repository KADoNiS at low kT, leading to a reduction in the cerium abundance predicted by the FUNS stellar model, regardless of the star metallicity. This measurement will help in identifying potential observational biases in current Galactic disk surveys. The high cerium abundance in globular clusters remains a mystery. A possible solution comes from the intermediate neutron capture process, but it requires additional theoretical work and the measurement of the neutron capture cross section of the unstable  $^{140}\text{Ba}$ , which are outside the scope of this work.

The cerium oxide material for this measurement has been provided by Professor T. Katabuchi of the Tokyo Institute of Technology. The authors thank M. Pignatari for massive star calculations and useful discussions.

I. U. R. acknowledges support from the U.S. National Science Foundation (Grants No. AST 1613536, No. AST 1815403/1815767, No. AST 2205847, and No. PHY 1430152—Joint Institute for Nuclear Astrophysics—Chemical Evolution of the Elements). S. C. acknowledges funding by the European Union—NextGenerationEU RFF M4C2 1.1 PRIN 2022 project “2022RJLWHN URKA” and by INAF Theory Grant “Understanding R-process & Kilonovae Aspects (URKA).” The authors acknowledge support from the MSMT of the Czech Republic, the Charles University UNCE/SCI/013 project, and by the funding agencies of the participating institutes. The authors declare that they have no known competing financial interests or personal relationships that could have appeared to influence the work reported in this Letter.

\*Deceased

- [1] E. M. Burbidge, G. R. Burbidge, W. A. Fowler, and F. Hoyle, Synthesis of the elements in stars, *Rev. Mod. Phys.* **29**, 547 (1957).
- [2] F. Käppeler, R. Gallino, S. Bisterzo, and W. Aoki, The s process: Nuclear physics, stellar models, and observations, *Rev. Mod. Phys.* **83**, 157 (2011).
- [3] M. Busso, R. Gallino, and G. J. Wasserburg, Nucleosynthesis in asymptotic giant branch stars: Relevance for galactic enrichment and solar system formation, *Annu. Rev. Astron. Astrophys.* **37**, 239 (1999).
- [4] O. Straniero, R. Gallino, and S. Cristallo, s process in low-mass asymptotic giant branch stars, *Nucl. Phys.* **A777**, 311 (2006).
- [5] F. Herwig, Evolution of asymptotic giant branch stars, *Annu. Rev. Astron. Astrophys.* **43**, 435 (2005).
- [6] A. I. Karakas and J. C. Lattanzio, The dawes review 2: Nucleosynthesis and stellar yields of low- and intermediate-mass single stars, *Pub. Astron. Soc. Aust.* **31**, e030 (2014).
- [7] O. Straniero, S. Cristallo, and L. Piersanti, Heavy elements in globular clusters: The role of asymptotic giant branch stars, *Astrophys. J.* **785**, 77 (2014).
- [8] I. U. Roederer, A. F. Marino, and C. Sneden, Characterizing the heavy elements in globular cluster M22 and an empirical s-process abundance distribution derived from the two stellar groups, *Astrophys. J.* **742**, 37 (2011).
- [9] I. Dillmann, F. Käppeler, R. Plag, and T. Rauscher, KADoNiS v0.3—The Karlsruhe Astrophysical Database of Nucleosynthesis in Stars, *AIP Conf. Proc.* **819**, 123 (2006).
- [10] F. Käppeler, K. A. Toukan, M. Schumann, and A. Mengoni, Neutron capture cross sections of the cerium isotopes for s- and p-process studies, *Phys. Rev. C* **53**, 1397 (1996).
- [11] S. Harnood, M. Igashira, T. Matsumoto, S. Mizuno, and T. Ohsaki, Measurement of keV-neutron capture cross sections and capture gamma-ray spectra of  $^{140}\text{Ce}$  and  $^{141}\text{Pr}$ , *J. Nucl. Sci. Technol.* **37**, 740 (2000).
- [12] A. R. D. L. Musgrove, B. J. Allen, and R. L. Macklin, Resonance neutron capture in  $^{138}\text{Ba}$  and  $^{140}\text{Ce}$  and the prompt neutron correction to  $\gamma$ -ray detectors, *Aust. J. Phys.* **32**, 213 (1979).
- [13] M. Ohkubo, M. Mizumoto, and Y. Nakajima, JAERI-M Reports No. 93-012, 1993.
- [14] C. Guerrero *et al.*, Performance of the neutron time-of-flight facility n\_TOF at CERN, *Eur. Phys. J. A* **49**, 27 (2013).
- [15] R. Plag, M. Heil, F. Käppeler, P. Pavlopoulos, R. Reifarth, and K. Wisshak, An optimized  $\text{C}_6\text{D}_6$  detector for studies of resonance-dominated ( $n, \gamma$ ) cross-sections, *Nucl. Instrum. Methods Phys. Res., Sect. A* **496**, 425 (2003).
- [16] S. Marrone *et al.* (n\_TOF Collaboration), A low background neutron flux monitor for the n\_TOF facility at CERN, *Nucl. Instrum. Methods Phys. Res., Sect. A* **517**, 389 (2004).
- [17] P. Schillebeeckx, B. Becker, Y. Danon, K. Guber, H. Harada, J. Heyse, A. R. Junghans, S. Kopecky, C. Massimi, M. C. Moxon, N. Otuka, I. Sirakov, and K. Volev, Determination of resonance parameters and their covariances from neutron induced reaction cross section data, *Nucl. Data Sheets* **113**, 3054 (2012).
- [18] S. Agostinelli *et al.*, GEANT4—a simulation toolkit, *Nucl. Instrum. Methods Phys. Res., Sect. A* **506**, 250 (2003).
- [19] R. Macklin, J. Halperin, and R. Winters, Absolute neutron capture yield calibration, *Nucl. Instrum. Methods Phys. Res., Sect. A* **164**, 213 (1979).
- [20] D. Brown *et al.*, Endf/b-viii.0: The 8th major release of the nuclear reaction data library with cielo-project cross sections, new standards and thermal scattering data, *Nucl. Data Sheets* **148**, 1 (2018), special Issue on Nuclear Reaction Data.
- [21] O. Iwamoto *et al.*, Japanese evaluated nuclear data library version 5: JENDL-5, *J. Nucl. Sci. Technol.* **60**, 1 (2023).
- [22] K. Guber, G. Alaerts, J. Heyse, S. Kopecky, C. Paradela Dobarro, P. Schillebeeckx, and W. R., Results of time-of-flight transmission measurements for natce samples at gelina, [10.2789/3763](https://arxiv.org/abs/10.2789/3763) (2016).
- [23] See Supplemental Material at <http://link.aps.org/supplemental/10.1103/PhysRevLett.132.122701> for resonance parameters for  $^{140}\text{Ce}$  for neutron energies lower than 65 keV.
- [24] S. Mughabghab, *Atlas of Neutron Resonances (Sixth Edition)* (Elsevier, Amsterdam, 2018).
- [25] A. Carlson *et al.*, Corrigendum to “evaluation of the neutron data standards” [nucl. data sheets 148, p. 143 (2018)], *Nucl. Data Sheets* **163**, 280 (2020).
- [26] S. Cristallo, O. Straniero, R. Gallino, L. Piersanti, I. Domínguez, and M. T. Lederer, Evolution, nucleosynthesis, and yields of low-mass asymptotic giant branch stars at different metallicities, *Astrophys. J.* **696**, 797 (2009).
- [27] S. Cristallo, L. Piersanti, O. Straniero, R. Gallino, I. Domínguez, C. Abia, G. Di Rico, M. Quintini, and S. Bisterzo, Evolution, nucleosynthesis, and yields of low-mass asymptotic giant branch stars at different metallicities. II. The FRUITY database, *Astrophys. J. Suppl. Ser.* **197**, 17 (2011).
- [28] D. Vescovi, S. Cristallo, M. Busso, and N. Liu, Magnetic-buoyancy-induced mixing in AGB stars: Presolar SiC grains, *Astrophys. J. Lett.* **897**, L25 (2020).
- [29] D. Vescovi, S. Cristallo, S. Palmerini, C. Abia, and M. Busso, Magnetic-buoyancy-induced mixing in AGB stars: Fluorine nucleosynthesis at different metallicities, *Astron. Astrophys.* **652**, A100 (2021).



- [30] D. Vescovi, Mixing and magnetic fields in asymptotic giant branch stars in the framework of FRUITY models, *Universe* **8**, 16 (2021).
- [31] N. Prantzos, C. Abia, S. Cristallo, M. Limongi, and A. Chieffi, Chemical evolution with rotating massive star yields II. A new assessment of the solar s- and r-process components, *Mon. Not. R. Astron. Soc.* **491**, 1832 (2020).
- [32] M. P. Roriz, M. Lugaro, C. B. Pereira, C. Sneden, S. Junqueira, A. I. Karakas, and N. A. Drake, Heavy elements in barium stars, *Mon. Not. R. Astron. Soc.* **507**, 1956 (2021).
- [33] C. M. Sakari *et al.*, The R-process alliance: First release from the northern search for r-process-enhanced metal-poor stars in the galactic halo, *Astrophys. J.* **868**, 110 (2018).
- [34] G. Contursi, P. de Laverny, A. Recio-Blanco, E. Spitoni, P. A. Palicio, E. Poggio, V. Grisoni, G. Cescutti, F. Matteucci, L. Spina, M. A. Álvarez, G. Kordopatis, C. Ordenovic, I. Oreshina-Slezak, and H. Zhao, The cerium content of the Milky Way as revealed by Gaia DR3 GSP-Spec abundances, *Astron. Astrophys.* **670**, A106 (2023).
- [35] Abdurro'uf *et al.*, The seventeenth data release of the sloan digital sky surveys: Complete release of MaNGA, MaStar, and APOGEE-2 data, *Astrophys. J. Suppl. Ser.* **259**, 35 (2022).
- [36] S. Buder *et al.* (Galah Collaboration), The GALAH + survey: Third data release, *Mon. Not. R. Astron. Soc.* **506**, 150 (2021).
- [37] M. Pignatari, R. Gallino, G. Meynet, R. Hirschi, F. Herwig, and M. Wiescher, The s-process in massive stars at low metallicity: The effect of primary  $^{14}\text{N}$  from fast rotating stars, *Astrophys. J. Lett.* **687**, L95 (2008).
- [38] U. Frischknecht, R. Hirschi, M. Pignatari, A. Maeder, G. Meynet, C. Chiappini, F.-K. Thielemann, T. Rauscher, C. Georgy, and S. Ekström, s-process production in rotating massive stars at solar and low metallicities, *Mon. Not. R. Astron. Soc.* **456**, 1803 (2016).
- [39] M. Pignatari, R. Hirschi, M. Wiescher, R. Gallino, M. Bennett, M. Beard, C. Fryer, F. Herwig, G. Rockefeller, and F. X. Timmes, The  $^{12}\text{C} + ^{12}\text{C}$  reaction and the impact on nucleosynthesis in massive stars, *Astrophys. J.* **762**, 31 (2013).
- [40] J. J. Cowan and W. K. Rose, Production of  $^{14}\text{C}$  and neutrons in red giants., *Astrophys. J.* **212**, 149 (1977).
- [41] M. Hampel, A. I. Karakas, R. J. Stancliffe, B. S. Meyer, and M. Lugaro, Learning about the intermediate neutron-capture process from lead abundances, *Astrophys. J.* **887**, 11 (2019).